the GaAlAs layer. Zn diffusion is performed at 600°C for 15 min to form a low resistance ohmic base contact. Ni-AuGe is used for emitter and collector contacts, and Ni-AuZn for the base contact.

The I/V characteristic of the transistor is shown in Fig. 2. An emitter–collector breakdown voltage V_{CEO} of 80 V was reached. The relatively high breakdown voltage of the emitter junction, roughly 40 V, is caused by its low doping level. Current gains h_{fe} ranging from 20 to 300 indicate an electron diffusion length of about 5 ~ 7 μm.

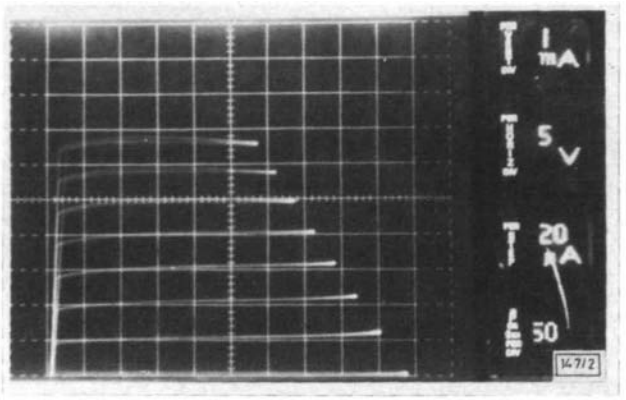

Fig. 2 *Static I/V characteristics of GaAlAs/GaAs heterojunction microwave bipolar transistor*

Fig. 3 shows the h_{fe}/I_C characteristic; uniform gain extends over a wide current range from 10 μA to 100 mA. The maximum collector current I_{Cm} of the transistor is about 150 mA to 200 mA, which together with the high breakdown voltage V_{CEO} implies a possible high power capability.

The maximum frequency of oscillation f_{max} measured from the S-parameters is 850 MHz (V_{CE} = 20 V, I_C = 20 mA), and the cutoff frequency f_T is deduced to be 1·6 GHz. Both are limited mainly by a relatively high emitter contact resistance R_e (≃ 20 Ω), although, to our knowledge, this is the best performance so far reported.[3,4]

Fig. 4 shows the equivalent circuit of the transistor; the two junction capacitances are measured by C/V measurements at 1 MHz. A rather low base–collector junction capacitance of 2 pF is the result of the low doping level (3×10^{15} cm^{-3}) in the collector layer. The emitter inductance L_e is calculated to

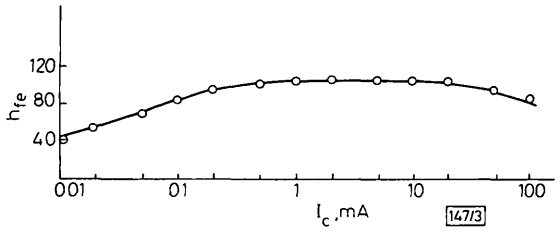

Fig. 3 h_{fe}/I_C *behaviour of transistor*
V_{CE} = 10 V; $A_E = 2 \times 10^{-4}$ cm^2

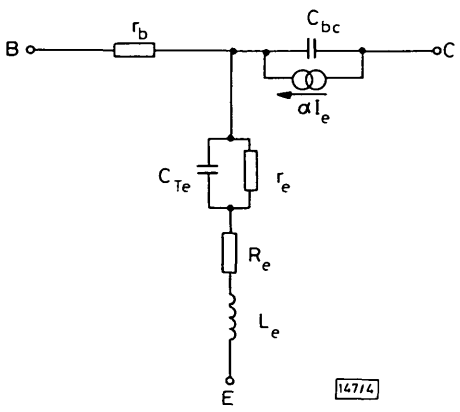

Fig. 4 *Equivalent circuit of transistor*
V_{CE} = 20 V; I_C = 20 mA
$r_e = nkT/qI_E$ (n = 1·5 ~ 2)
r_b = 2 Ω, C_{Te} = 15 pF, C_{bc} = 2 pF,
α = 0·95 ~ 0·99, R_e = 20 Ω, L_e = 1 nH (d = 20 μm, l = 1 mm)

be 1 nH by assuming the bonding wire length of 1 mm with its diameter of 20 μm.

The current gain h_{fe} versus temperature is shown in Fig. 5; the gain drops gradually as the temperature rises, reaching about one third of its maximum value at 350°C case temperature. The corresponding emitter–collector reverse current I_{CEO} was measured at V_{CE} = 10 V to be 400 μA. These results are much better than for any existing Ge or Si transistors.

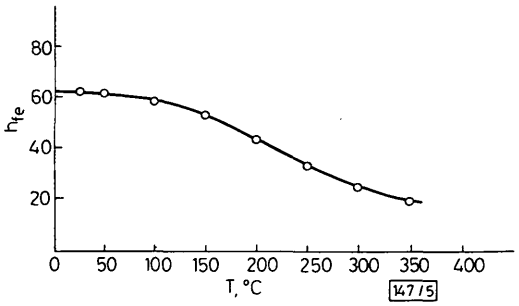

Fig. 5 h_{fe}*/temperature characteristic for heterojunction transistor*
V_{CE} = 10 V; I_C = 10 mA

Acknowledgment: The authors are indebted to R. Stahlmann, who performed the S-parameter measurements, F. Ponse for his skilful technical assistance and J. Knauf for help in fabrication.

H. BENEKING
L. M. SU

Institute of Semiconductor Electronics
Aachen Technical University
Templergraben 55, D-5100 Aachen, West Germany

17th March 1981

References

1 KROEMER, H.: 'Theory of a wide gap emitter for transistor', *Proc. IRE*, 1957, **45**, pp. 1535–1537
2 DUMKE, W. P., WOODALL, J. M., and RIDEOUT, V. L.: 'GaAs-GaAlAs heterojunction transistor for high frequency operation', *Solid-State Electron.*, 1972, **15**, pp. 1339–1343
3 ANKRI, D., and SCAVENNEC, A.: 'Design and evaluation of a planar GaAlAs/GaAs bipolar transistor', *Electron. Lett.*, 1980, **16**, pp. 41–42
4 BAILBE, J. P., MARTY, A., HIEP, P. H., and REY, G. E.: 'Design and fabrication of high-speed GaAlAs/GaAs heterojunction transistors', *IEEE Trans.*, 1980, **ED-27**, pp. 1160–1164

0013-5194/81/080301-02$1.50/0

HISTOGRAM EQUALISATION WITH S AND π FUNCTIONS IN DETECTING X-RAY EDGES

Indexing terms: Pattern recognition, Image processing

An algorithm consisting of a histogram equalisation technique followed by further enhancement using S and π membership functions is described to detect the small variation in grey levels of X-ray images. The effectiveness of the algorithm in identifying the different regional contours related to growth of normal bones is demonstrated.

Introduction: Histogram equalisation[1,2] is a widely used and well established strategy for enhancing images like X-ray pictures and landscape photographs that are taken under poor illumination. This technique results in an increase in the dynamic range of the pixels by 'stretching' of their grey scale (which increases the contrast). The higher the contrast, the better is the edge detection.

X-ray images of hand and wrist consist of a number of regions relating to small variations in grey level corresponding to

soft tissue, single bone, superimposed bones, palmar and dorsal surfaces[3] (which appear with growth of a child) and other three dimensional effects of bones. In such cases, when the number of regions is large, the contrast between these successive regions even after the application of the histogram equalisation technique remains insufficient to detect their edges. This letter presents an algorithm which uses S and π functions and INT operator[4] on the histogram-equalised image such that the pixels of every alternate region would undergo a similar kind of enhancement keeping the dynamic range constant. As a result, the grey tone contrast between successive regions tends to be significant.

Histogram equalisation technique: If r_l and n_l denote the value of the lth grey level and the number of times the lth level has appeared respectively in an $M \times N$, L-level image array $X = \{x_{mn}: m = 1, 2, \ldots, M; n = 1, 2, \ldots, N\}$, then the transformation[1]

$$s_l = T(r_l) = \frac{L-1}{MN} \sum_j n_j; \quad j = 0, 1, 2, \ldots, l; \quad l = 0, 1, 2, \ldots, L-1 \quad (1)$$

which is equal to the cumulative distribution of r_l, will result in a modified value s_l from the original level r_l. The distribution of s_l will give the resulting equalised histogram.

S and π membership functions: The graphical representation of the $\pi(x_{mn}; l_2 - l_1, l_c)$ membership function for providing the p_{mn} value ($0 \leq p_{mn} \leq 1$) corresponding to pixel intensity x_{mn}, $0 \leq x_{mn} \leq x_{max}$ ($= L - 1$) is shown in Fig. 1. Here l_1 and l_2 denote the crossover points (at which $\pi = 0{\cdot}5$), $l_c = (l_1 + l_2)/2 = x_{max}/2$ and $(l_2 - l_1)$ is the bandwidth Δl. The left part of the Figure corresponds to an S-function between zero and $x_{max}/2$, whereas the right part is represented by a $(1 - S)$-function within the interval $[x_{max}/2, x_{max}]$.

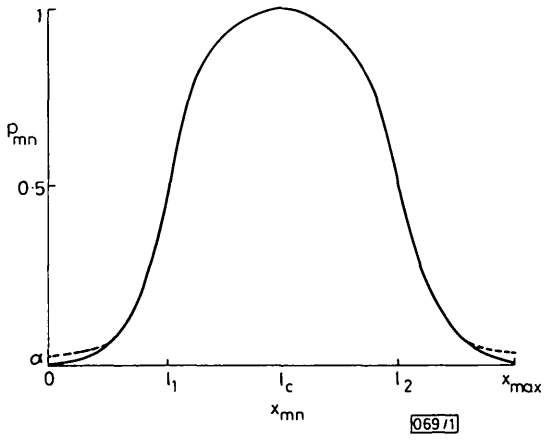

Fig. 1 *G_π-function*

To represent both these functions, we define

$$p_{mn} = G(x_{mn}) = [1 + |\hat{x} - x_{mn}|/F_d]^{-F_e}; \quad m = 1, 2, \ldots, M; \quad n = 1, 2, \ldots, N \quad (2)$$

The positive constants F_e and F_d control the crossover points, bandwidth and hence the symmetry of the curve about the crossover points. $\hat{x}$ is the reference constant such that the function (eqn. 2) is[5]

S-type (G_S): for $\hat{x} = x_{max}$

π-type (G_π): for $\hat{x}$ = some other level l_c, $0 < l_c < x_{max}$

The functions G_S and G_π represent the compatibility functions corresponding to image planes 'x_{mn} is x_{max}' and 'x_{mn} is l_c', respectively. The corresponding p_{mn} values denote the degree of possessing maximum brightness level x_{max} and some other level l_c by the (m, n)th pixel x_{mn}. α is the value of p_{mn} for $|\hat{x} - x_{mn}| = \hat{x}$ (Fig. 1).

Contrast intensification in p_{mn}-plane: The contrast between two/three consecutive regions corresponding to S/π-type p_{mn}-plane is increased by the r ($= 1, 2, \ldots$) successive uses of the fuzzy INT (contrast intensification) operator[4] which is defined by the recursive relationship

$$p'_{mn} = T_r(p_{mn}) = T_1\{T_{r-1}(p_{mn})\} \quad (3)$$

where

$$T_1(p_{mn}) = T'_1(p_{mn}) = 2p_{mn}^2 \qquad 0 \leq p_{mn} \leq 0{\cdot}5 \quad (4a)$$

$$= T''_2(p_{mn}) = 1 - 2(1 - p_{mn})^2 \qquad 0{\cdot}5 \leq p_{mn} \leq 1 \quad (4b)$$

As r increases, p'_{mn} values for the regions 0 to l_1 and l_1 to l_2 (for G_S-plane) would approach zero and unity respectively, whereas for G_π-plane, it would approach unity for the region l_1 to l_2 and zero for the rest (Fig. 1).

Extension to k (> 3) successive regions: The above concept can then be extended to the isolation of more than 3 regions by the successive use of S or π functions over the regions in question.

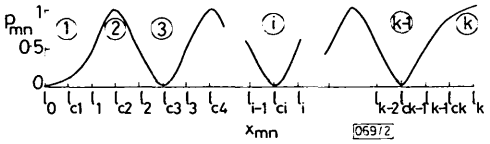

Fig. 2 *G_W-function; alternate use of G_π and $(1 - G_\pi)$*

Fig. 2 shows such an application of G_π and its complement $(1 - G_\pi)$ to enhance the contrast level among k regions ranging from l_0 to l_k in the spatial domain. Let $l_1, l_2, \ldots, l_{k-1}$ be the intensities of the $(k - 1)$ boundary levels between these regions. Then we use

$$p_{mn} = G_W(x_{mn}) = G_\pi(x_{mn}; l_2 - l_1, l_{c2}) \qquad x_{mn} \leq l_2 \quad (5a)$$

$$= 1 - G_\pi(x_{mn}; l_3 - l_2, l_{c3}) \qquad l_2 \leq x_{mn} \leq l_3 \quad (5b)$$

$$= 1 - G_\pi(x_{mn}; l_{k-1} - l_{k-2}, l_{c(k-1)}) \qquad x_{mn} \geq l_{k-2} \quad (5c)$$

where

$$\Delta x_k = l_k - l_{k-1}; \quad l_{ck} = (l_k + l_{k-1})/2 \quad (6)$$

Eqn. 5c is based on the assumption that k is even. If k is odd, it will be G_π. Again in practice, the bandwidths Δx_i, $i = 1, 2, \ldots, k$, may be all different. After applying the T_r operation (eqns. 3 and 4) on this G_W-plane, the resulting p'-domain would contain k separable regions with a value $\ll 0{\cdot}5/\gg 0{\cdot}5$ corresponding to $\Delta x_i/\Delta x_{i+1}$, $i = 1, 2, \ldots$.

Inverse membership function: After the enhanced p'_{mn}-domain is

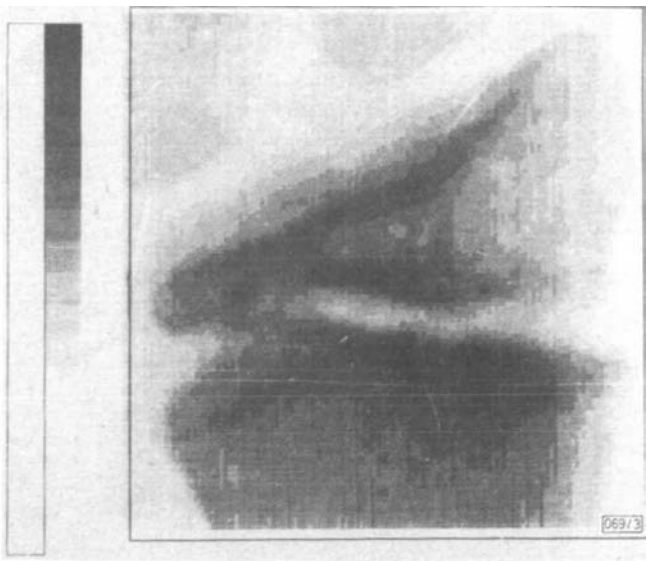

Fig. 3 *Input image*

produced by $G_W(x_{mn}) \rightarrow T_r(p_{mn})$ transformation, we use

$$x'_{mn} = G_S^{-1}(p'_{mn})|_{\hat{x}=x_{max};\, l_i=x_{max}/2} \qquad \alpha \leq p'_{mn} \leq 1$$

to obtain the corresponding contrast intensified spatial domain x'_{mn}. Since the $G_S^{-1}(p'_{mn})$ (unlike G_π^{-1}) yields a single valued x'_{mn}-domain whose dynamic range is determined by $\hat{x}$ and the symmetry about the crossover point is determined by F_e and F_d, the above transformation will generate a symmetrical spatial domain of full dynamic range (0 to x_{max}). The resulting image X' would have values either $x'_{mn} \gg x_{max}/2$ or $\ll x_{max}/2$ corresponding to $p'_{mn} \gg 0{\cdot}5$ and $\ll 0{\cdot}5$ in the alternate regions. The contrast (difference in grey level) between any two consecutive regions of X' would therefore approach x_{max}.

Implementation and results: Fig. 3 shows an 128 × 145, 256-level image of a wrist containing radius (with epiphysis and metaphysis) and a part of two small carpal bones of a boy of 10–12 years. The input image contains 5 regions approximating to (i) 50 to 80, (ii) 80 to 100, (iii) 100 to 135, (iv) 135 to 165, and (v) 165 to 200. The first and last regions correspond to soft tissue, and palmar and dorsal surfaces respectively. The increase in dynamic range of the equalised image (as obtained with eqn. 1) has changed these regions to (i) 0 to 20, (ii) 20 to 65, (iii) 65 to 150, (iv) 150 to 215, and (v) 215 to 255, respectively. The five contrast-intensified regions as obtained after the transformation $G_W(x_{mn}) \rightarrow T_r(p_{mn}) \rightarrow G_S^{-1}(p'_{mn})$ are shown in Fig. 4. Here we have used $r = 4$ and the values of F_d for $F_e = 2$ were considered to be 53·113, 102·601 and 76·041 so that the crossover points l_1, l_2, l_3 and l_4 can correspond to 20·5, 64·5, 149·5 and 212·5, respectively. The l values were determined from the equalised histogram. Fig. 5 demonstrates the grey level edges using a detector; the (m, n)th edge $\triangleq |x'_{mn} - \min_Q \{x'_{ij}\}|$, where Q is a set of four nearest neighbours x'_{ij} of x'_{mn}.

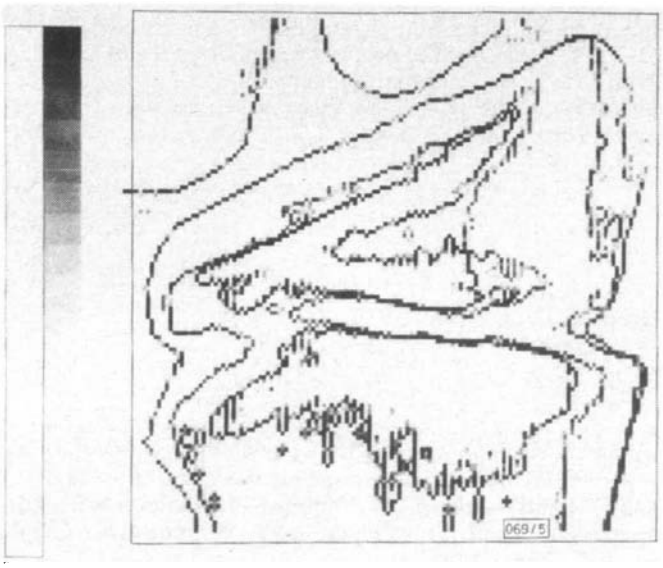

Fig. 4 *Five contrast-intensified regions*

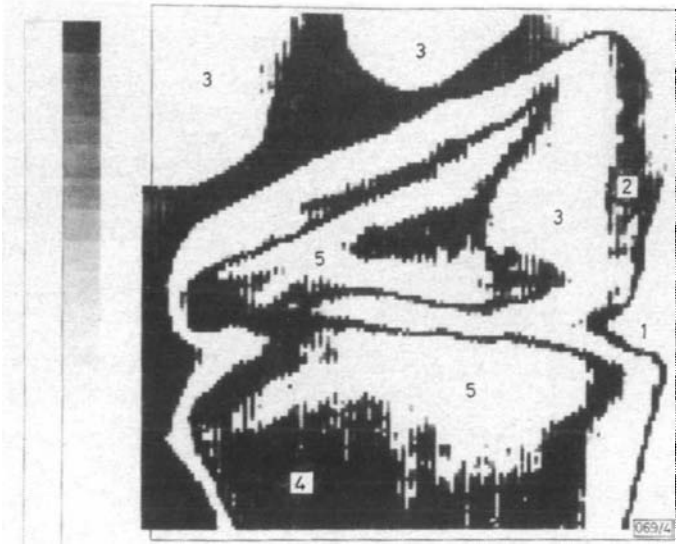

Fig. 5 *Grey tone edges*

S. K. PAL†
R. A. KING

Electrical Engineering Department
Imperial College of Science & Technology
London SW7 2BT, England

19th February 1981

† On leave from Electronics and Communication Sciences Unit, Indian Statistical Institute, Calcutta 700 035, India.

References

1 GONZALEA, R. C., and WINTZ, P.: 'Digital image processing' (Addison-Wesley, London, 1977)
2 'Picture processing', *Philips Tech. Rev.*, 1979/80, **38**, (11/12)
3 TANNER, J. M., *et al.*: 'Assessment of skeletal maturity and prediction of adult height (TW2 method)' (Academic Press, NY, 1975)
4 ZADEH, L. A., *et al.* (EDS.): 'Fuzzy sets and their applications to cognitive and decision processes' (Academic Press, London, 1975)
5 PAL, S. K., and KING, R. A.: 'Image enhancement using fuzzy set', *Electron. Lett.*, 1980, **16**, pp. 376–378

0013-5194/81/080302-03$1.50/0

OPTICAL TEE COUPLER FOR DATA BUS SYSTEM WITH SINGLE MULTIMODE FIBRES

Indexing terms: Optical communications, Optical connectors

A new type of optical tee coupler was developed for a data bus system with single multimode fibres. It is constructed of a wedge-shaped mirror and three graded-index rod lenses. Its three ports, which are ready to plug in, interconnect asymmetrically with one another. For a laser diode of wavelength 0·9 μm, the coupling losses between three fibres attached into the ports were adjusted to be 3·9 to 7·9 dB. The coupler insertion losses were 1·3 to 2·5 dB.

Introduction: As compared with conventional coaxial cables, optical fibres have desirable features such as large transmission capacity and lack of electromagnetic interference and ground loop problems. The potential advantages of fibres have led to a great interest in adopting fibre optic transmission systems in electric power systems or industrial plants.[1,2] In such applications, single-fibre data bus systems, in which many spatially distributed terminals are served with the same multiplexed signal, are very suitable. There are two generic approaches to the multiterminal data bus systems: the star approach and the more conventional tapped trunk line (tee-system) approach. In the approaches based on fibre bundles, some kinds of star or tee couplers have been reported.[3,4] However, they have a very serious limitation of high coupling losses at the interface

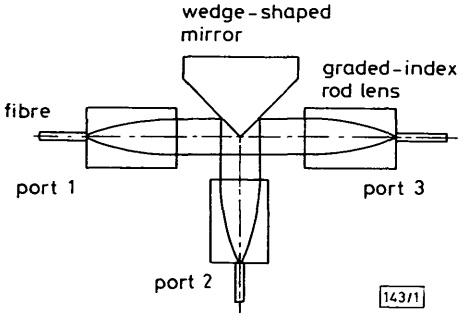

Fig. 1 *Schematic diagram of tee coupler*